Int J Cardiovasc Imaging (2011) 27:385–396
DOI 10.1007/s10554-010-9672-6

ORIGINAL PAPER

Geometry and dimensions of the pulmonary artery bifurcation in children and adolescents: assessment in vivo by contrast-enhanced MR-angiography

Zita Knobel · Christian J. Kellenberger · Thomas Kaiser · Manuela Albisetti · Eva Bergsträsser · Emanuela R. Valsangiacomo Buechel

Received: 19 December 2009 / Accepted: 8 July 2010 / Published online: 21 July 2010

Abstract We sought to establish normal values for the diameters of the main (MPA), right (RPA), and left (LPA) pulmonary arteries and for the angles describing the geometry of the pulmonary artery bifurcation in children by using contrast-enhanced magnetic resonance angiography (CE-MRA). CE-MRA was performed in 69 children without cardiovascular disease. The median age was 10 ± 4.9 years (range 2–20), weight 37.4 ± 18.5 kg (10–82), body surface area (BSA) 1.18 ± 0.4 m^2 (0.48–2.07). The pulmonary artery diameters and angles were measured at standardized sites and projections. Regression analysis of diameters and angles in relation to BSA demonstrated linear relationship between the cross-sectional diameters of the pulmonary arteries and the square root of BSA ($BSA^{0.5}$). Normalized mean diameters were for the MPA 17.6 ± 5.1 mm/m^2, origin of RPA 13.1 ± 2.9 mm/m^2, origin of LPA 14.2 ± 2.9 mm/m^2. The MPA showed a mean antero-posterior inclination of 33° ± 8° and a lateral left-ward angulation of 18° ± 5°. The mean angle of the bifurcation was 99.5° ± 10.3°. Both side branches showed a supero-inferior course of the proximal segments, steeper for the RPA (7.7° ± 6.5°) than for the LPA (2.1° ± 7.8°). Normative curves in relation to BSA are presented for all measurements. This study provides normative values by CE-MRA for the main pulmonary artery and its side branches in children during somatic growth. These data can be used for identifying pulmonary arteries anomalies in children, and evaluate the need and the modality for treatment.

Keywords Pulmonary arteries · Congenital heart disease · Children · Cardiovascular magnetic resonance imaging · Angiography

Z. Knobel · T. Kaiser · E. R. Valsangiacomo Buechel (✉)
Division of Pediatric Cardiology, University Children's Hospital, Steinwiesstrasse 75, 8032 Zurich, Switzerland
e-mail: emanuela.valsangiacomo@kispi.uzh.ch

C. J. Kellenberger
Department of Diagnostic Imaging, University Children's Hospital, Zurich, Switzerland

M. Albisetti
Division of Haematology, University Children's Hospital, Zurich, Switzerland

E. Bergsträsser
Division of Pediatric Oncology, University Children's Hospital, Zurich, Switzerland

Introduction

The right-sided cardiac structures, including the pulmonary valve, main pulmonary artery (MPA) and pulmonary artery side branches (PAs) are often involved in congenital heart disease (CHD). Besides the intrinsic malformation of the pulmonary vasculature, additional factors such as chronic hypoxia may have influence on its development [1, 2]. Nowadays, thanks to the enormous progress of congenital cardiac

surgery during the last decade, even the most complex malformations can be potentially corrected with good results [3, 4]. When complete reconstruction of the pulmonary artery bifurcation is necessary the surgeon should attempt to reconstruct the pulmonary pathways harmoniously copying the natural geometry of the bifurcation, in order to avoid distortion of the vessels and steep angles, which may cause turbulent flow and growth disturbance of the vessels [5]. Nevertheless, postoperative residual anomalies of the PAs are not uncommon and are among the most frequent causes for reintervention [6, 7]. Moreover, the size of the PAs is being used as predictor for the postoperative outcome of specific procedures, such as the Fontan operation [8, 9].

Data about the normal size of the PAs in children have been established in the past by using autoptic data, echocardiographic and angiographic studies [10–15]. Information about the geometry of the pulmonary artery bifurcation and about the course of the proximal segments of the PAs remains scarce.

Cardiovascular magnetic resonance (CMR) represents the ideal technique for studying both the size of a vascular structure and its geometric configuration within the body, as it can be performed in vivo, it is non-invasive and provides 3-dimensional information. The accuracy of CMR angiographic measurements compared to conventional angiographic measurements has been previously demonstrated [16]. Thus CMR is being increasingly integrated in the diagnostic and therapeutic pathways of patients with complex CHD, and routinely used for planning surgical or catheter-guided reinterventions [17, 18].

Knowledge of the normal values for the PAs assessed by CMR is essential for grading the severity of anomalies, defining the need for and planning an intervention.

Aim of the study was to assess the normal geometry and the size of the MPA and its side branches during growth, by using contrast-enhanced CMR angiography (CE-MRA).

Methods

Subjects

Seventy-seven children with previous history of a malignancy underwent CE-MRA for assessment of potential port-a-cath related complications. All subjects were required to have normal cardiovascular anatomy, no evidence of cardiovascular disease and normal body size, according to normative data for the Swiss population [19]. Five children with a body size above the 97% percentile, and 3 with insufficient image quality were excluded from the study. Patients who had previous chest radiation therapy or tumor related conditions such as anemia, ongoing chemotherapy or treatments affecting the cardiovascular loading conditions were excluded from the study.

The Ethics Committee of our institution approved the study protocol. Written informed consent allowing additional analysis of the image data for this study was obtained from the children's parents or a legal guardian.

Technique

All CMR examinations were performed on a 1.5-T Sigma MR/i Twinspeed scanner (GE Medical Systems, Milwaukee, Wisconsin, USA) with the smallest coil allowing coverage of the neck and the chest (i.e. quadrature head coil, different sized multichannel phased-array surface coils). CE-MRA was performed using a 3D fast spoiled gradient echo sequence (3D FSPGR) with linear k-space filling, flip angle 30°, bandwith ± 62 kHz, repetition time 3.2–3.4 ms, and echo time 0.9–1.1 ms. The field of view (260–480 mm), slice thickness (2–3.2 mm), and number of partitions (26–48) were adjusted to the child's size. A matrix of 256 × 160 and zero interpolation in all three axes (ZIP 512, ZIP 4) provided a spatial resolution ranging from 0.5 × 0.5 × 0.8 mm^3 to 0.8 × 0.9 × 1.5 mm^3. A double dose (0.2 mmol/kg bodyweight, maximum dose 20 ml) of Gadolinium-based contrast medium (dimeglumine gadopentate, Magnevist®, Bayer AG, Switzerland; or gadodiamide, Omniscan®, GE Healthcare AG, Switzerland) was injected intravenously as a bolus over 10 s with a power injector (Medrad Spectris, Pittsburgh, USA), and flushed with the same volume of saline solution and the same injection rate. Image acquisition was timed to the first pass of the contrast medium through the aorta by measuring the contrast travel time (T_C) to the descending aorta with a real-time two-dimensional FSPGR sequence and a test bolus of 1 ml contrast material. The individual start delay of the 3D FSPGR

acquisition was calculated as follows: $T_D = T_C - T_{Ac}/2 + 5$, where T_D is the time delay (in seconds) between the start of the contrast material injection and data acquisition, and T_{Ac} is the 3D data acquisition time. Because the primary purpose of the CE-MRA was assessment of the systemic veins, the 3D data acquisition was repeated 3 times.

Children under sedation with propofol ($n = 22$) and those not able to hold their breath ($n = 2$) were imaged during quiet breathing, while the other children ($n = 45$) were imaged during three consecutive breathholds of 20 s duration.

Sedation was induced intravenously with propofol 2 mg/kg and further doses of 1 mg/kg as necessary. Meticulous care was taken to maintain spontaneous breathing. Oxygen in a dose of 2 l/min was applied with a nasal cannula with separate O_2 tube and CO_2 sampling tube (Salter Labs, Arvin, California). Deep sedation was continued with propofol 10 mg/kg h given as continuous intravenous infusion, following our institutional protocol. Routine monitoring of capnography with respiratory rate and end-tidal carbon dioxide concentration, oxygen saturation, heart rate, electrocardiogram and blood pressure, was assessed continuously (Datex-Ohmeda MRA Monitor, Datex-Ohmeda, Helsinki, Finland).

Image reconstruction and measurements

CE-MRA source data were reconstructed on a commercially available off-line workstation (SUN Microsystems Inc., Mountain View, CA, USA). From the acquired sets of images, the one with the highest signal in the pulmonary arteries was selected for reconstruction. Maximum intensity projection (MIP) images were obtained using reformatting software (Volume analysis 2, Voxtool 3.051f, GE medical Systems, Milwaukee, Wisconsin, USA).

Images were reconstructed in five standardized projections as shown in Fig. 1.

(1) An axial view through the pulmonary artery bifurcation was prescribed from both a coronal and sagittal image (Fig. 1a).
(2) A right anterior oblique view (RAO) was obtained by setting a plane along the midline of the right pulmonary artery (RPA) on the axial image (Fig. 1b).
(3) A left anterior oblique view (LAO) was obtained by setting a plane along the midline of the left pulmonary artery (LPA) on the axial image (Fig. 1c).
(4) A sagittal oblique view was obtained by tailoring a plane through the midline of the MPA on the axial and coronal images (Fig. 1d).

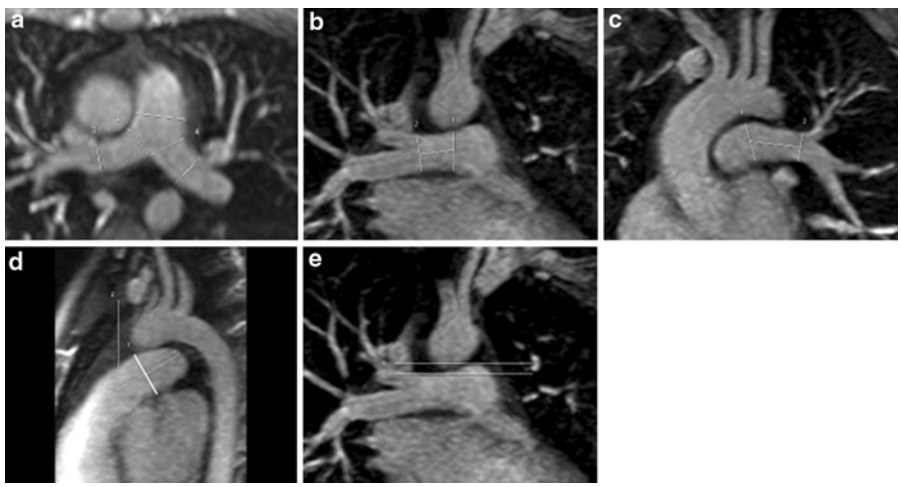

Fig. 1 Reconstructed MIP images and sites of measurements. **a** *Axial view* with diameter measurements of the MPA, proximal and distal RPA and LPA. **b** *Right anterior oblique view* with measurements of the proximal (*1*) and distal (*2*) RPA diameters, as well as of the distance to the origin of the first segmental artery branch. **c** *Left anterior oblique view* with measurements of the proximal (*1*) and distal (*2*) LPA diameters, as well as of the distance to the origin of the first segmental artery branch. **d** *Sagittal oblique view* with measurement of the MPA diameter and of the angle of inclination. **e** Coronal view with measurement of the offset between the origins of the LPA and RPA

(5) A coronal view at the level of both PAs was prescribed from a sagittal image, for demonstrating the offset of their origins (Fig. 1e).

The locations of the measurements are also shown in Fig. 1. The diameters of the MPA were measured perpendicular to the vessel, midway between the pulmonary valve and the bifurcation, in the axial and the sagittal oblique views. The proximal diameters of the RPA and LPA were defined as the diameters at the origin of the vessels at the pulmonary bifurcation, and were measured in the axial and the RAO and LAO views, respectively (Fig. 1a–c). The length of the proximal segment of the RPA and LPA was defined as the distance between the origin and the first segmental branching of the upper lobe in each artery, and measured on the respective coronal oblique views, RAO and LAO (Fig. 1b, c).

The course of the MPA was defined as its lateral and anterior-posterior angulation in relation to the sagittal and horizontal planes through the chest; we measured the angles between the midline of the MPA and a sagittal plane on the axial image (Fig. 2a) and between the midline of the MPA and a horizontal plane on the sagittal oblique image (Fig. 1d), respectively. The geometry of the pulmonary artery bifurcation was defined by measuring the total angle between the posterior borders of the RPA and LPA as well as separate angles for the RPA and LPA in relation to the midline of the MPA Fig. 2b). In addition, the superior-inferior course of the PAs was assessed as the angle between a horizontal line at the level of the bifurcation and a midline through the RPA and LPA on the respective coronal oblique view (Fig. 2c, d).

The offset of the RPA and LPA origins was measured on a coronal view as the distance between horizontal lines drawn at the upper borders of the RPA and LPA origins (Fig. 1e).

Statistical analysis

Continuous data are expressed as mean ± standard deviation (SD) or median and range as appropriate. The diameters of the vessels were indexed to the body surface area (BSA) according to the Mosteller formula [20]. Differences in angles between RPA and LPA were tested using the paired *t*-test. *P*-values <0.05 were considered to be statistically significant.

Regression analysis was performed, as previously suggested for vessel diameters, in relation to the square root of BSA [21–23], by using linear functions, polynomial first and polynomial second order functions. The best statistical model was defined by a high r^2 value and by analysis of the residuals [22].

Intra- and interobserver variability was assessed in 15 randomly selected patients with the Bland–Altman analysis of the mean difference and the limits of agreement between measurements [24]. For intraobserver variability the same observer (Z.K.) repeated

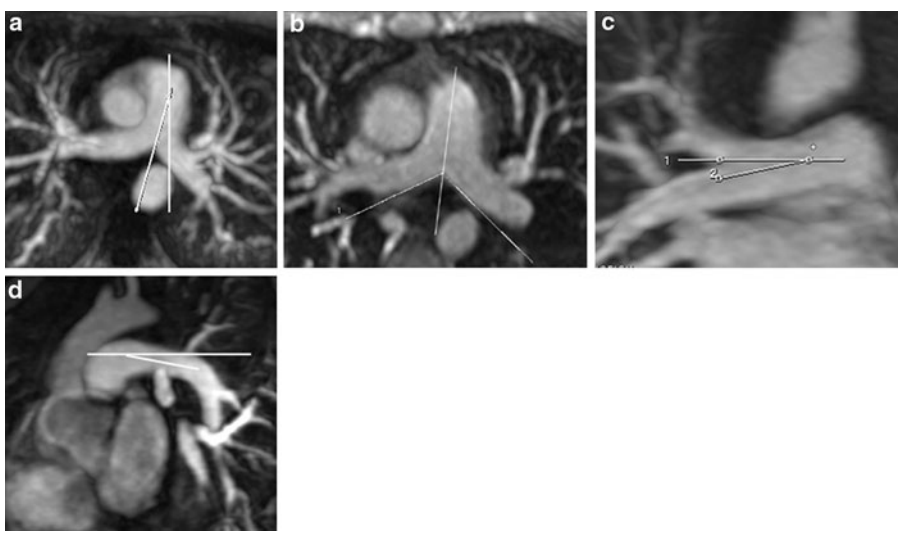

Fig. 2 Angle measurements on MIP images. **a** *Axial view*. Lateral angulation of the MPA. **b** *Axial view*. Bifurcation angles. **c** *RAO view* Cranio-caudal angulation of the RPA. **d** *LAO view*. Cranio-caudal angulation of LPA

the measurements after an interval of several months. The interobserver variability was assessed by comparison of the results by two independent observers (Z.K., E.R.V.).

Statistical analysis was performed using a commercially available software package (Prism 4.03, GraphPad Software Inc., San Diego, USA).

Results

Sixty-nine children (28 female, 41 male) were included in the study. The median age was 10 ± 4.9 years (range 2–20 years), body weight was 37.4 ± 18.5 kg (range 10–82 kg), and height was 138 ± 27 cm (range 81–188 cm). The median BSA was 1.14 ± 0.4 m^2 (range 0.48–2.07 m^2). Age ($P = 0.67$), weight ($P = 0.33$) and height ($P = 0.35$) did not differ significantly between female and male subgroups.

Diameters

The diameters of the MPA, RPA and LPA, and the distances between the origin and the first branches of the RPA and LPA are presented in Table 1. A linear relationship between the diameters of the PAs and the square root of BSA ($BSA^{0.5}$) was the best fitting model for regression (diameter = a + b*$BSA^{0.5}$). The regression equations are listed in Table 2 and the corresponding curves in relation to BSA are shown in the Figs. 3, 4, and 5.

Table 1 Diameters of the pulmonary arteries

Diameters	Mean ± SD (mm)
MPA axial	17.6 ± 5.1
MPA sagittal	17.5 ± 4.3
RPAp axial	11.4 ± 3.1
RPAd axial	9.8 ± 2.9
RPAp RAO	13.1 ± 2.9
RPAd RAO	13.0 ± 2.9
LPAp axial	12.5 ± 3.0
LPAd axial	11.3 ± 2.5
LPAp LAO	14.2 ± 2.9
LPAd LAO	11.1 ± 2.1

MPA main pulmonary artery, *RPAp* proximal right pulmonary artery, *RPAd* distal right pulmonary artery, *LPAp* proximal left pulmonary artery, *LPAd* distal left pulmonary artery, *RAO* right anterior oblique view, *LAO* left anterior oblique view

Table 2 Functions of normal diameters (diameter = a + b*$BSA^{0.5}$)

Site	Predicted diameter (mm)	Standard deviation of residuals (mm)
MPA axial	4.85 + 13.43*$BSA^{0.5}$	2.72
MPA sagittal	1.04 + 17.07*$BSA^{0.5}$	2.01
RPAp axial	2.63 + 9.19*$BSA^{0.5}$	1.65
RPAd axial	3.9 + 6.25*$BSA^{0.5}$	1.49
RPAp RAO	−0.69 + 14.3*$BSA^{0.5}$	1.76
RPAd RAO	−1.08 + 14.62*$BSA^{0.5}$	1.6
LPAp axial	1.7 + 11.27*$BSA^{0.5}$	1.37
LPAd axial	−0.1 + 11.89*$BSA^{0.5}$	1.51
LPAp LAO	−2.13 + 16.82*$BSA^{0.5}$	1.88
LPAd LAO	−2.08 + 13.64*$BSA^{0.5}$	1.5

MPA main pulmonary artery, *RPAp* proximal right pulmonary artery, *RPAd* distal right pulmonary artery, *LPAp* proximal left pulmonary artery, *LPAd* distal left pulmonary artery, *RAO* right anterior oblique view, *LAO* left anterior oblique view

The mean length of the proximal segment of the RPA was 17 ± 6.5 mm, of the LPA 14.8 ± 4.9 mm ($P < 0.001$).

Angles

The MPA showed an oblique course from right anterior inferior to left posterior superior with an angle of mean 18° ± 5.5° to the left (Fig. 6a) and with an anterior-posterior inclination of 33° ± 8°.

The mean total angle of the pulmonary artery bifurcation measured 99° ± 10° (Fig. 2b), with angulation of the pulmonary artery side branches in relation to the MPA axis of 47° ± 7° for the RPA and 52° ± 8° for the LPA ($P < 0.001$).

The offset between the origins of RPA and LPA measured 6.7 ± 2.2 mm.

Both pulmonary artery side branches showed a superior-inferior course with a mean cranio-caudal angle in relation to a horizontal plane of 8° ± 6° for the RPA and of 2° ± 8° for the LPA (Fig. 6b). Thus the course of the RPA was significantly steeper than that of the LPA ($P < 0.001$). None or very weak correlation was found between the angles and BSA.

The results of inter- and intraobserver variability analysis are listed in Table 3.

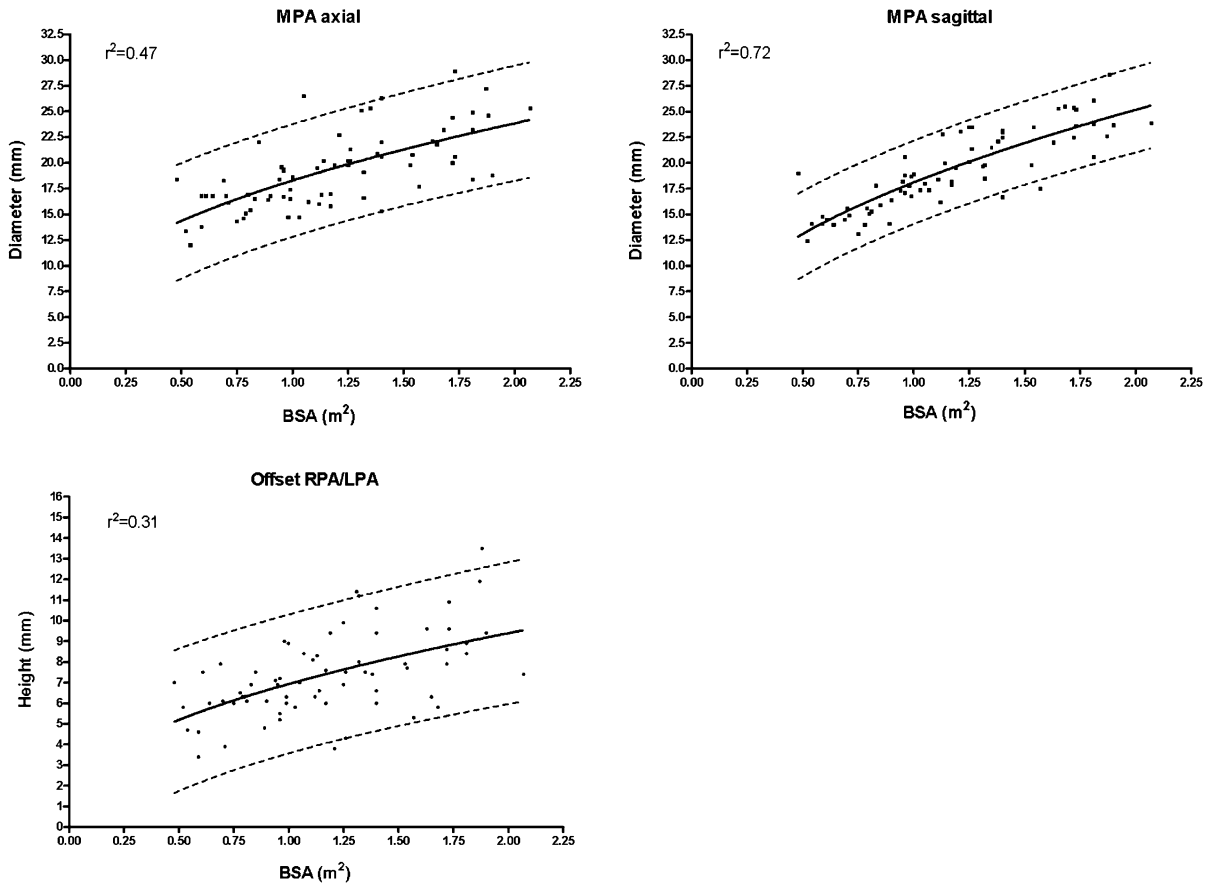

Fig. 3 Linear regression curves with 95% prediction bands for the MPA diameters and offset of the origin of the side branches versus BSA

Discussion

This study provides data on the normal diameter of the MPA and its proximal side branches and on the geometry of the pulmonary bifurcation in children and adolescents. The data has been acquired in vivo with the technique of CE-MRA.

The normal dimensions of the PAs, assessed by different methods, including angiography, echocardiography and autoptic measurements, are available in the literature [11–15, 25]. However, to our knowledge the position of the PAs within the chest and the geometry of the pulmonary artery bifurcation have not yet been described in vivo.

Knowledge about the normal range of the pulmonary vascular morphology is important in congenital cardiology, as anomalies of the PAs are common concomitant findings in congenital lesions affecting the right size of the heart. In addition, PAs can be dilated in presence of a relevant intracardiac shunt [11]; the dimensions of the PAs are sometimes used for risk stratification or as predictor for prognosis [9]. Finally, when a cardiac defect has been repaired, prompt recognition of residual findings such as diminutive PAs, distortion of the vascular geometry, and failure to growth may be essential for further management.

The results of this study are potentially of unique interest for surgeons and interventional cardiologists, focussing their attention on the ideal vascular geometry to be targeted. In fact, after the recent dramatic improvement of surgical techniques for repair of complex CHD, the next goal may be to refine anatomical reconstruction of the PAs in order to

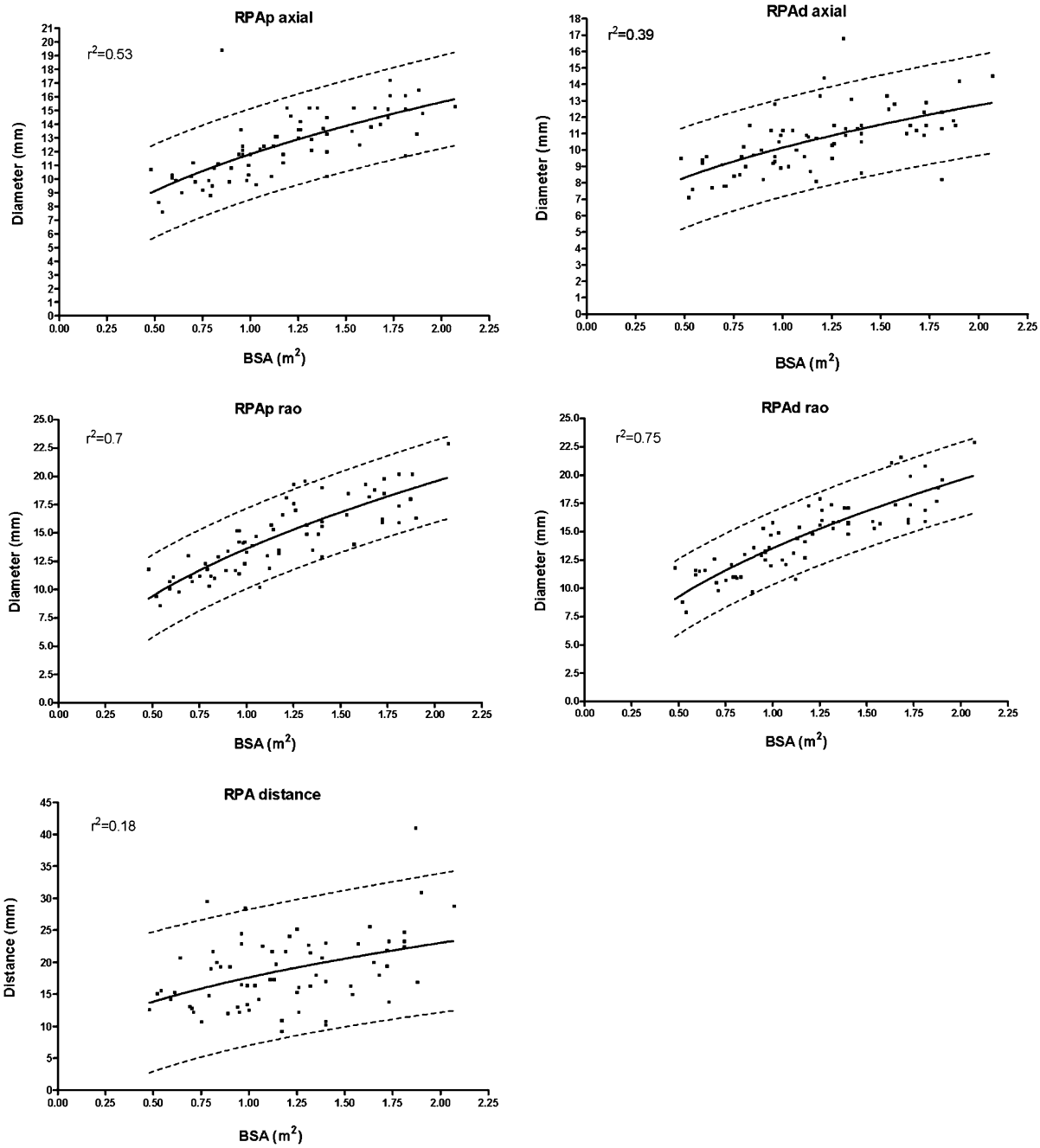

Fig. 4 Linear regression curves with 95% prediction bands for the RPA diameters and distance to origin of first segmental artery branch versus BSA

achieve an almost normal anatomy. At time of vascular reconstruction, the importance of the branching angles and branch artery diameters should be taken into account [26]. The diameters and the branching angles of the PAs determine four physiologic entities, so called "cost functions", consisting of (1) the pumping power required to drive blood through an arterial bifurcation, (2) the total drag force exercised by the flowing blood on endothelial tissue, (3) the total lumen and (4) the total lumen surface of the bifurcation.

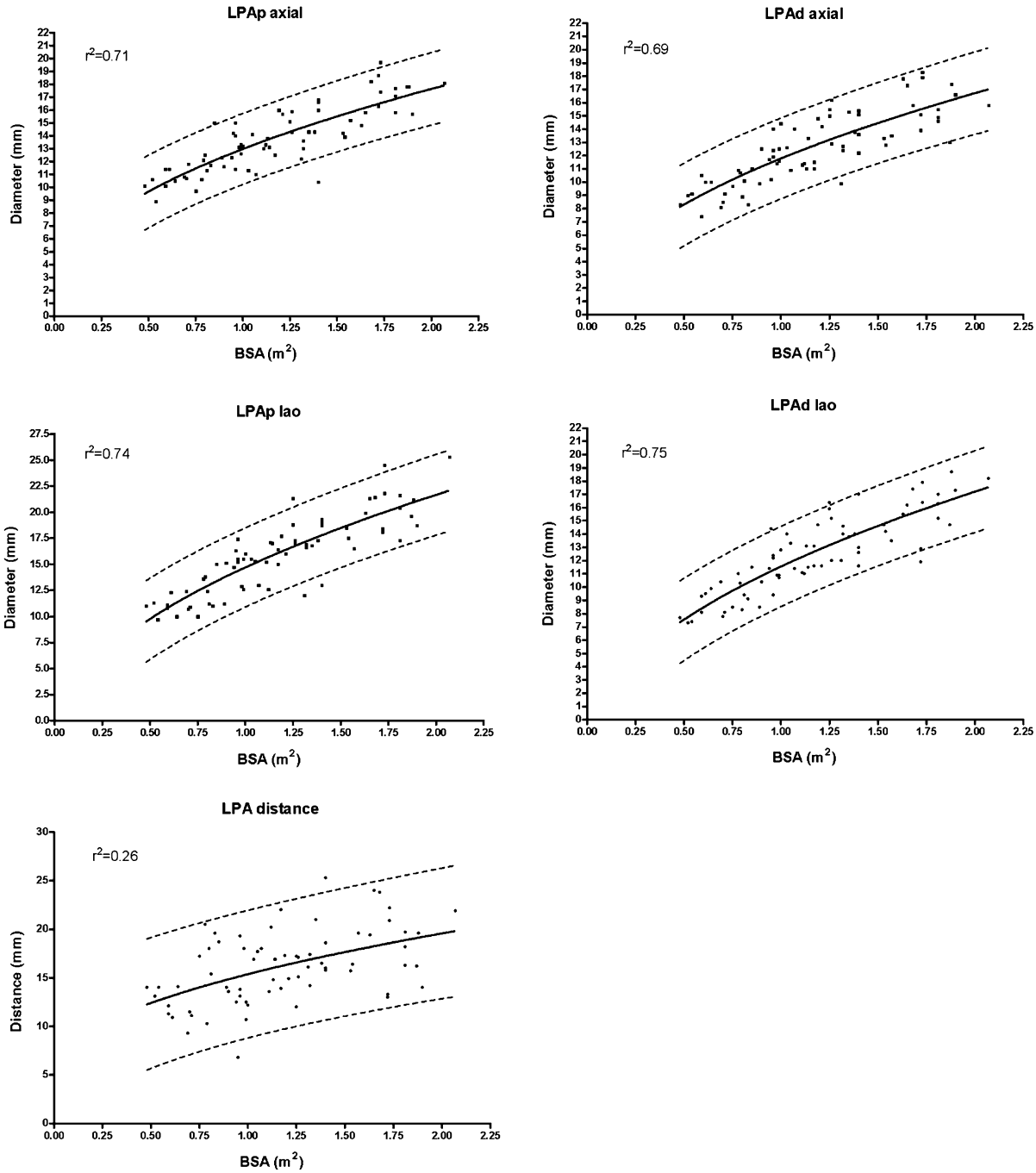

Fig. 5 Linear regression curves with 95% prediction bands for the LPA diameters and distance to first segmental artery branch versus BSA

The optimal branching angles are those that produce the minimal value of cost function [27]. This principle of minimum work is even more important in CHD, where small improvements in the physiological efficiency may results in large effects on mid- and long-term outcome parameters, such as longer lasting right ventricular function or appropriate growth of the pulmonary vasculature.

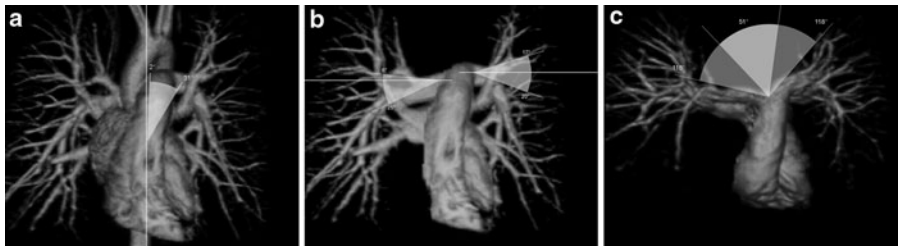

Fig. 6 3D volume rendered images illustrating the normal geometry of the pulmonary artery bifurcation with the range of measured angles. **a** *Anterior view* showing the course of the MPA from *right inferior* to *left superior* (angle range 2°–31°). **b** *Anterior view* showing the cranio-caudal course of the RPA (range 25° caudally–6° cranially) and of the LPA (range 20° caudally–17° cranially). **c** *Superior view* showing the angle of bifurcation (range 51°–118°)

Table 3 Intra- and interobserver variability

Variables ($n = 15$)	Mean (mm)	Intraobserver variability		Interobserver variability	
		Mean difference ± SD	Limits of agreement	Mean difference ± SD	Limits of agreement
Diameters					
MPA axial	18.7	0.2 ± 1.0	−1.8/+ 2.1	−0.3 ± 0.7	−1.7/+ 1.2
MPA sagittal	18.4	−0.1 ± 0.6	−1.3/+ 1.0	0.1 ± 1.4	−2.8/+ 2.9
RPAp axial	12.2	0.0 ± 0.7	−1.4/+ 1.4	−0.1 ± 0.8	−1.8/+ 1.6
RPAd axial	10.6	0.4 ± 0.8	−1.3/+ 2.1	0.5 ± 0.7	−1/+ 1.9
RPAp RAO	13.8	0.2 ± 0.5	−0.8/+ 1.3	0.7 ± 1.5	−2.3/+ 3.7
RPAd RAO	14.2	0.2 ± 0.8	−1.4/+ 1.9	0.3 ± 0.6	−0.9/+ 1.5
LPAp axial	13.7	−0.1 ± 0.7	−1.4/+ 1.3	0.0 ± 0.8	−1.6/+ 1.5
LPAd axial	12.9	−0.1 ± 0.9	−1.9/+ 1.6	0.0 ± 0.9	−1.9/+ 1.9
LPAp LAO	15.3	0.1 ± 0.7	−1.4/+ 1.5	−0.1 ± 0.6	−1.3/+ 1.1
LPAd LAO	11.9	0.3 ± 0.6	−0.8/+ 1.5	0.1 ± 0.9	−1.6/+ 1.8
Distances					
RPA prox.segment	18	1.5 ± 2.7	−3.0/+ 6.9	1.2 ± 2.2	−3.2/+ 5.6
LPA prox.segment	16.3	0.9 ± 2.6	−4.2/+ 6	1.0 ± 2.4	−3.7/+ 5.8
Offset RPA/LPA	7.4	−1.1 ± 1.0	−3.0/+ 0.9	−0.6 ± 1.2	−2.9/+ 1.8
Angles					
Bifurcation	98.7	1.5 ± 5.6	−9.8/+ 12.7	0.9 ± 4.8	−8.7/+ 10.4
MPA axial	18.1	1.5 ± 2.0	−2.4/+ 5.4	−4.8 ± 2.5	−9.8/+ 0.2
MPA sagittal	59.7	0.5 ± 3.7	−6.9/+ 7.8	2.4 ± 5.9	−9.4/+ 14.2
RPA axial	47.6	−1.9 ± 4.6	−11.1/+ 7.2	4.7 ± 3.6	−2.6/+ 11.9
RPA RAO	−7.6	−0.5 ± 2.0	−4.4/+ 3.4	0.5 ± 5.7	−10.9/+ 12
LPA axial	50.7	2.7 ± 2.8	−3/+ 8.3	−3.7 ± 3.8	−11.3/+ 4
LPA LAO	−3.1	−0.4 ± 2.3	−5/+ 4.2	−1.1 ± 2.8	−6.6/+ 4.5

MPA main pulmonary artery, *RPAp* proximal right pulmonary artery, *RPAd* distal right pulmonary artery, *LPAp* proximal left pulmonary artery, *LPAd* distal left pulmonary artery, *RAO* right anterior oblique view, *LAO* left anterior oblique view

CE-MRA, thanks to its well-known advantages, is being increasingly used in centres specialized in treatment of CHD during clinical decision making and for planning surgical or catheter-guided interventions [16, 17]. Therefore, availability of specific normal values for this particular technique is essential; we chose imaging planes similar to the views used for conventional angiography.

The use of BSA as expression of body size in children and the use of linear regression models to describe the relationship between body growth and the cardiovascular dimensions have been previously validated [12, 21, 22]. Thus similar to other authors for angiography [15, 25] and echocardiography [11, 12], we found a non linear relationship between body growth and the dimensions of the pulmonary arteries that we described by using a linear regression equation containing $BSA^{0.5}$, as suggested by Sluysmans et al. [22]. The regression coefficients found in our study were more similar to those reported for angiography by Rammos et al. and Sievers et al. [14, 25], then those reported in echocardiographic studies by Snider et al. and Lappen et al. [11, 12]. This can be explained by the fact that methodological differences in image acquisition, particularly the planes and projections, are more pronounced between echocardiography and other angiographic techniques, in our study conventional angiography and CE-MRA, then among the angiographic techniques themselves. The slight differences observed among different studies are potentially the result of known expected differences by using different imaging modalities [14, 22]. In general, diameters measured in one single projection, or not exactly perpendicularly to the vessel course, as it may be the case by using echocardiography or conventional angiography, may introduce methodical inaccuracy. Moreover the data published for echocardiography were acquired during diastole, yielding to smaller diameters compared to measures performed during systole [12]. Similarly, Rammos et al. found a difference of 10% between systolic and diastolic diameters of the Pas [14], and Sievers et al. suggested to use an average between both measurements [25]. CE-MRA images represent an average between both cardiac phases, systole and diastole; we previously demonstrated the accuracy of CE-MRA measurements compared to conventional angiography [16]. CE-MRA overcomes the limitations of image acquisition in both other modalities; by using MIP reconstruction and the double-oblique technique, the diameters can be accurately measured perpendicular to the vessel. Moreover by assessing the diameters and the angulation in 2 planes for each vessel, we attempted to provide three-dimensional information.

In the literature we found no description of the relationship between somatic growth and the geometry of the PAs. Our data show a large variability of the geometry of the PAs in normal children, with a wide range of angle values and distances between the bifurcation and the origins of the first segmental artery branches. Even by testing different regression models, we were not successful in demonstrating a significant correlation between the angles and BSA.

The results of intra- and interobserver variability confirm very high repeatability of the CE-MRA measurements of vascular diameters and distances [16]. Variability was slightly higher for measurement of angles, but still within the accepted limit of 10%.

Limitations

The power of this study may be limited by its relatively small sample size, and by the fact that only children with a BSA larger than 0.48 m^2 were included. Even though a linear correlation between vascular diameters and $BSA^{0.5}$ has been described also for very small children, and such a regression curve could be potentially extrapolated from our data, we recommend caution for the use of our normogramms for children smaller than 0.5 m^2.

The analysis of our measurements did not show any significant difference for males and females. For this reason all data are presented on the same graph, independently from gender. Nevertheless, a gender difference could potentially be found in a larger study population.

Ethical considerations prevented the use of contrast medium in healthy children. For this reason the study was planned in patients undergoing CMR for evaluation of potential port-a-cath complications, who may not represent an entirely normal population. We endeavoured to eliminate any potential bias to the subject's characteristics, by selecting the participants in accordance with strict selection criteria and with the help of our colleague oncologists. Thus all children who received a treatment protocol, which may had potential direct or indirect influence on growth or haemodynamics of the intrathoracic cardiovascular system were excluded from the study.

Conclusions

This study provides normal values for the diameters of the pulmonary arteries and for the geometry of the

pulmonary bifurcation in children. CE-MRA allows description of the normal anatomy of the great vessels in vivo with high reproducibility of the measurements.

This data may be useful for planning surgical or catheter-guided interventions for repair of CHD, for postoperative assessment of the further development of the pulmonary arteries and for risk stratification before selected operations.

Acknowledgment We thank Dr. Luciano Molinari for the statistical support.

References

1. Rabinovitch M, Herrera-deLeon V, Castaneda AR, Reid L (1981) Growth and development of the pulmonary vascular bed in patients with tetralogy of Fallot with or without pulmonary atresia. Circulation 64(6):1234–1249
2. Rabinovitch M, Reid LM (1981) Quantitative structural analysis of the pulmonary vascular bed in congenital heart defects. Cardiovasc Clin 11(2):149–169
3. Duncan BW, Mee RBB, Prieto LR, Rosenthal GL, Mesia CI, Qureshi A, Tucker OP, Rhodes JF, Latson LA (2003) Staged repair of tetralogy of Fallot with pulmonary atresia and major aortopulmonary collateral arteries. J Thorac Cardiovasc Surg 126(3):694–702. doi:10.1016/S0022-5223(03)00700-1
4. Reddy VM, McElhinney DB, Amin Z, Moore P, Parry AJ, Teitel DF, Hanley FL (2000) Early and intermediate outcomes after repair of pulmonary atresia with ventricular septal defect and major aortopulmonary collateral arteries: experience with 85 patients. Circulation 101(15):1823–1832
5. Kaczmarek I, Schmauss D, Reichart B, Daebritz SH (2006) Complete autologous reconstruction of the aorta and the pulmonary bifurcation in truncus arteriosus communis. Eur J Cardiothorac Surg 30(4):675–677. doi:10.1016/j.ejcts.2006.06.033
6. Oechslin EN, Harrison DA, Harris L, Downar E, Webb GD, Siu SS, Williams WG (1999) Reoperation in adults with repair of tetralogy of fallot: indications and outcomes. J Thorac Cardiovasc Surg 118(2):245–251
7. Ishibashi N, Shin'oka T, Ishiyama M, Sakamoto T, Kurosawa H (2007) Clinical results of staged repair with complete unifocalization for pulmonary atresia with ventricular septal defect and major aortopulmonary collateral arteries. Eur J Cardiothorac Surg 32(2):202–208. doi:10.1016/j.ejcts.2007.04.022
8. Knott-Craig CJ, Julsrud PR, Schaff HV, Puga FJ, Danielson GK (1993) Pulmonary artery size and clinical outcome after the modified Fontan operation. Ann Thorac Surg 55(3):646–651
9. Senzaki H, Isoda T, Ishizawa A, Hishi T (1994) Reconsideration of criteria for the Fontan operation. Circulation 89(3):1196–1202
10. Gussenhoven WJ, van Leenen BF, Kuis W, de Villeneuve VH, Born N (1983) Comparison of internal diameter of great arteries in congenital heart disease. A cross-sectional echocardiographic study. Br Heart J 49(1):45–50. doi:10.1136/hrt.49.1.45
11. Lappen RS, Riggs TW, Lapin GD, Paul MH, Muster AJ (1983) Two-dimensional echocardiographic measurement of right pulmonary artery diameter in infants and children. J Am Coll Cardiol 2(1):121–126. doi:10.1016/s0735-1097(83)80384-2
12. Snider AR, Enderlein MA, Teitel DF, Juster RP (1984) Two-dimensional echocardiographic determination of aortic and pulmonary artery sizes from infancy to adulthood in normal subjects. Am J Cardiol 53(1):218–224
13. Van Meurs-van Woezik H, Debets T, Klein HW (1987) Growth of the internal diameters in the pulmonary arterial tree in infants and children. J Anat 151:107–115
14. Rammos S, Kramer HH, Trampisch HJ, Krogmann ON, Kozlik R, Bourgeois M (1989) Normal values of the growth of the pulmonary arteries in children—an angiography study. Herz 14:348–357
15. Rammos S, Apostolopoulou SC, Kramer HH, Kozlik-Feldmann R, Heusch A, Laskari CV, Anagnostopoulos C (2005) Normative angiographic data relating to the dimensions of the aorta and pulmonary trunk in children and adolescents. Cardiol Young 15(2):119–124. doi:10.1017/S1047951105000272
16. Valsangiacomo Büchel E, DiBernardo S, Bauersfeld U, Berger F (2005) Contrast-enhanced magnetic resonance angiography of the great arteries in patients with congenital heart disease: an accurate tool for planning catheter-guided interventions. Int J Cardiovasc Imaging 21(2–3):313–322. doi:10.1007/s10554-004-4017-y
17. Fratz S, Hess J, Schuhbaeck A, Buchner C, Hendrich E, Martinoff S, Stern H (2008) Routine clinical cardiovascular magnetic resonance in paediatric and adult congenital heart disease: patients, protocols, questions asked and contributions made. J Cardiovasc Magn Reson 10(1):46. doi:10.1186/1532-429X-10-46
18. Schievano S, Coats L, Migliavacca F, Norman W, Frigiola A, Deanfield J, Bonhoeffer P, Taylor A (2007) Variations in right ventricular outflow tract morphology following repair of congenital heart disease: implications for percutaneous pulmonary valve implantation. J Cardiovasc Magn Reson 9(4):687–695. doi:10.1080/10976640601187596
19. Prader L, Molinari I (1989) Wachstumskurven (Perzentilen). Helv Paediatr Acta Suppl 52:1–125
20. Mosteller RD (1987) Simplified calculation of body-surface area. N Engl J Med 317(17):1098
21. Kaiser T, Kellenberger C, Albisetti M, Bergsträsser E, Valsangiacomo Büchel E (2008) Normal values for aortic diameters in children and adolescents—assessment in vivo by contrast-enhanced MR-angiography. J Cardiovasc Magn Reson 10(1):56. doi:10.1186/1532-429X-10-56
22. Sluysmans T, Colan SD (2005) Theoretical and empirical derivation of cardiovascular allometric relationships in children. J Appl Physiol 99:445–457. doi:10.1152/japplphysiol.01144.2004
23. Gutgesell HP, Rembold CM (1990) Growth of the human heart relative to body surface area. Am J Cardiol 65(9):662–668

24. Bland JM, Altman DG (1986) Statistical methods for assessing agreement between two methods of clinical measurement. Lancet 1(8476):307–310
25. Sievers HH, Onnasch GGW, Lange P, Bernhard A, Heintzen PH (1983) Dimensions of the great arteries, semilunar valve root, and right ventricular outflow tract during growth: normative angiographic data. Pediatr Cardiol 4(3):189–196. doi:10.1007/BF02242254
26. Fanucci E, Orlacchio A, Pocek M (1988) The vascular geometry of human arterial bifurcations. Invest Radiol 23(10):713–718
27. Zamir M, Bigelow DC (1984) Cost of departure from optimality in arterial branching. J Theor Biol 109(3): 401–409. doi:10.1016/S0022-5193(84)80089-2